Quantum Origin of Limit Cycles, Fixed Points, and Critical Slowing Down

Shovan Dutta,[1,2] Shu Zhang,[1] and Masudul Haque[3,1]
[1]Max-Planck-Institut für Physik Komplexer Systeme, D-01187 Dresden, Germany
[2]Raman Research Institute, Bangalore 560080, India
[3]Institut für Theoretische Physik, Technische Universität Dresden, 01062 Dresden, Germany

(Received 4 June 2024; accepted 8 January 2025; published 7 February 2025)

Among the most iconic features of classical dissipative dynamics are persistent limit-cycle oscillations and critical slowing down at the onset of such oscillations, where the system relaxes purely algebraically in time. On the other hand, quantum systems subject to generic Markovian dissipation decohere exponentially in time, approaching a unique steady state. Here we show how coherent limit-cycle oscillations and algebraic decay can emerge in a quantum system governed by a Markovian master equation as one approaches the classical limit, illustrating general mechanisms using a single-spin model and a two-site lossy Bose-Hubbard model. In particular, we demonstrate that the fingerprint of a limit cycle is a slow-decaying branch with vanishing decoherence rates in the Liouville spectrum, while a power-law decay is realized by a spectral collapse at the bifurcation point. We also show how these are distinct from the case of a classical fixed point, for which the quantum spectrum is gapped and can be generated from the linearized classical dynamics.

DOI: 10.1103/PhysRevLett.134.050407

Introduction—The question of how classical behavior appears as an appropriate limit of quantum dynamics has intrigued physicists since the dawn of quantum mechanics [1–9]. For *Hamiltonian* classical systems, there is a distinction between chaotic and nonchaotic dynamics: a long line of work has explored the spectral manifestations of this distinction in corresponding quantum systems [10–23]. Non-Hamiltonian (dissipative) classical systems support far more intriguing nonlinear phenomena, such as limit cycles, bifurcations, period doubling transitions to chaos, and strange attractors [24,25]. However, a detailed understanding based on the quantum spectrum, at the level available for Hamiltonian systems, is currently missing in the dissipative case. The present work is a step toward formulating and addressing these questions.

A Markovian quantum dissipative system is described via a master equation $\dot{\rho} = \mathcal{L}\rho$ for the density matrix ρ, where the Liouvillian $\mathcal{L}$ is constrained to have the Lindblad or Gorini-Kossakowski-Sudarshan-Lindblad form [26–28]. Lindblad dynamics generally relax exponentially in time to a unique steady state, except in the case of special symmetries [29–32]. The behaviors at a classical limit cycle (persistent oscillations) and at bifurcation points (algebraic decay) appear to contradict this quantum description. Here, we show how such properties emerge from spectral features of $\mathcal{L}$ as the classical limit is approached. We illustrate our results primarily through a dissipative nonlinear spin model. To demonstrate that our findings are generic, we also illustrate some of these results using a driven-dissipative two-site Bose-Hubbard model [33–35].

Highlights of main results—Figure 1 shows schematics of the Liouvillian spectrum of a system approaching the classical limit that features a limit cycle (top panels) or its onset at a Hopf bifurcation (bottom panels). We focus on the low-lying (i.e., slow-decaying) part of the spectrum close to the imaginary axis. The spectral signature of a limit cycle is an approximately parabolic branch of eigenvalues including the steady state which collapses onto the imaginary axis in the classical limit, forming an equally spaced linear array. The eigenstates of this branch all have the same radial structure in classical phase space (concentrated around the limit cycle), but each has a different angular structure, $\sim e^{il\phi}$ with $l \in \mathbb{Z}$. The superposition of an infinite number of such states can yield a localized packet in phase space orbiting the limit cycle, recovering the classical late-time dynamics. Additionally, there are parallel branches that have weights at increasing radial distances with proportional decay rates.

At a Hopf bifurcation the classical dynamics features critical slowing down, relaxing algebraically in time. In contrast, in quantum Lindblad dynamics the decay to the steady state is generically exponential, governed by the real Liouvillian gap. This conflict is resolved through an infinite number of eigenvalues with the same angular but different radial structures collapsing on the imaginary axis in the

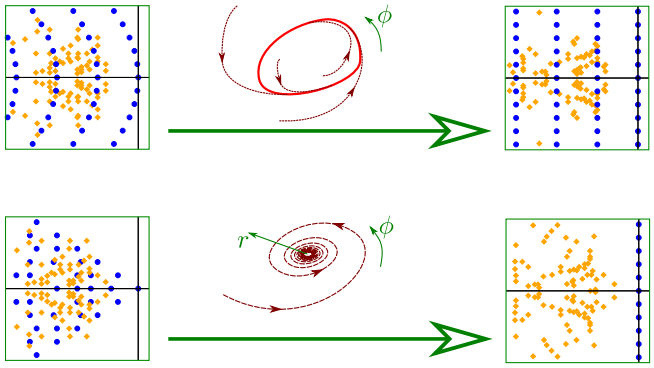

FIG. 1. Schematics illustrating the fate of Liouvillian spectra (left panels) in approaching the classical limit (right panels). For a limit cycle (top panels) the signature is a branch of equally spaced imaginary eigenvalues yielding coherent oscillations, plus gapped parallel branches, describing the approach to the limit cycle. The branches are parabolic in the quantum case, which causes dephasing at long times. At a Hopf bifurcation point (bottom panels) the spectrum collapses onto the imaginary axis, with macroscopic degeneracies at each harmonic, leading to algebraic decay. Additional eigenvalues, e.g., associated with other attractors in phase space, may exist, as indicated by the orange diamonds.

classical limit. This allows the radial approach to have a power-law form.

On the other side of the bifurcation, classical trajectories approach a stable fixed point. The quantum signature is a wedge-shaped array of Liouvillian eigenvalues [Figs. 2(c) and 2(e)] that follow from the classical Jacobian.

Spin model—We analyze a spin subject to a Zeeman field $\hat{H} = -\hat{S}_z$ and two competing quantum jump operators, $\hat{L}_1 = \hat{S}_+/\sqrt{S}$ and $\hat{L}_2 = \sqrt{\gamma/S^3}\hat{S}_-\hat{S}_z$. The former relaxes the spin toward the ground state at the north pole. The latter excites the spin away from it with a rate dependent on S_z; this nonlinearity is parametrized by the rate γ. The normalizations of $\hat{L}_j$ with factors of the spin length S guarantee consistency in the classical limit $S \to \infty$. In this limit, the Lindblad time evolution of the spin operators reduces to the following equations of motion on the unit (Bloch) sphere [36]:

$$\frac{\mathrm{d}s_z}{\mathrm{d}t} = (1-\gamma s_z^2)(1-s_z^2), \quad \frac{\mathrm{d}\phi}{\mathrm{d}t} = -1, \tag{1}$$

where $s_z \coloneqq \langle \hat{S}_z \rangle / S = \cos\theta$ and $\phi \coloneqq \arctan[\langle \hat{S}_y \rangle / \langle \hat{S}_x \rangle]$ can be regarded as classical variables. For $\gamma \leq 1$ all trajectories flow to a unique stable fixed point $s_z = 1$, whereas for $\gamma > 1$ a stable limit cycle at $s_z = 1/\sqrt{\gamma}$ coexists with a stable fixed point at $s_z = -1$, as shown in Figs. 2(a) and 2(b). At long times deviation from the final state decays exponentially for any $\gamma \neq 1$. The separation point $\gamma = 1$ features a Hopf bifurcation, at which the decay is algebraic, $s_z \approx 1 - 1/(4t)$.

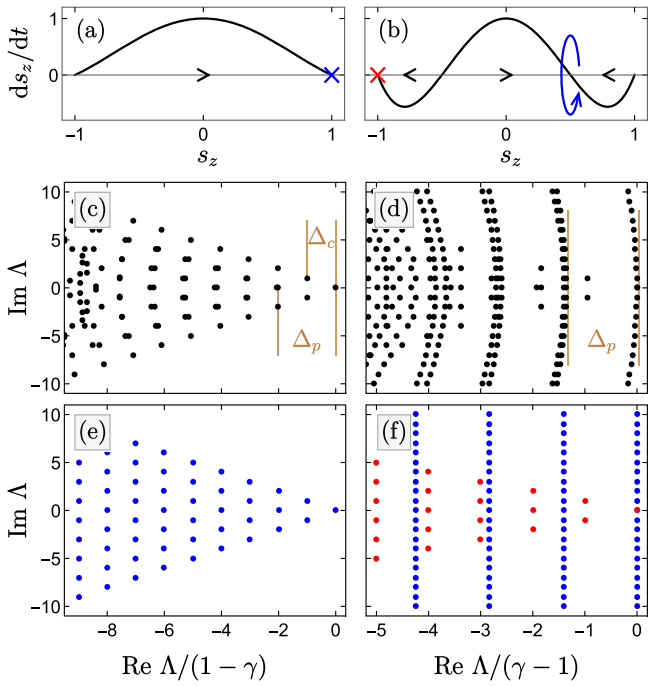

FIG. 2. (a),(b) Classical flow and (c)–(f) quantum spectra for the fixed point (left panels; $\gamma = 0.5 < 1$) and limit cycle (right panels; $\gamma = 2 > 1$) regimes of the spin model. (a),(b) Crosses are fixed points and the curved arrow denotes the limit cycle. (c),(d) Liouvillian spectra for $S = 300$. (e),(f) $S \to \infty$ spectrum from the semiclassical Fokker-Planck equation. In both regimes the gap Δ_p remains nonzero for $S \to \infty$, signifying the classical approach rate, whereas the gap Δ_c (decoherence rate) is nonzero for the fixed point but vanishes for the limit cycle. The blue and red dots in (f) correspond to the limit cycle and the coexisting fixed point at $s_z = -1$, respectively.

We now analyze the spectrum and dynamics of the quantum model, explaining how the classical dynamics is recovered. We will later argue that the major findings are generic (model independent). In addition to numerical solutions of the Liouvillian at finite S, we obtain complementary insights using a semiclassical limit of the Lindblad master equation [38,39]. The resulting Fokker-Planck equation for the phase-space distribution yields the exact spectrum of $\mathcal{L}$ in the $S \to \infty$ limit. For finite S it describes a wave packet that drifts along a classical trajectory and diffuses under quantum fluctuations.

Fixed-point regime—For $\gamma < 1$ the stable fixed point corresponds to the quantum steady state with eigenvalue $\Lambda = 0$ [Figs. 2(c) and 2(e)]. The steady state for finite S has a distribution of width $\Delta\theta \sim S^{-1/2}$ centered at the classical fixed point [Fig. 3(a)]. The rest of the spectrum is separated by a minimum real gap of Δ_c that approaches the classical decay rate $1-\gamma$ as $S \to \infty$.

In fact, in the classical limit the low-lying (small-$|\mathrm{Re}\,\Lambda|$) spectrum, which governs the late-time dynamics, is fully determined by the classical attractor. As shown in Fig. 2(e), the eigenvalues have the form $\sum_{j=1,2} n_j \lambda_j$, where n_j are

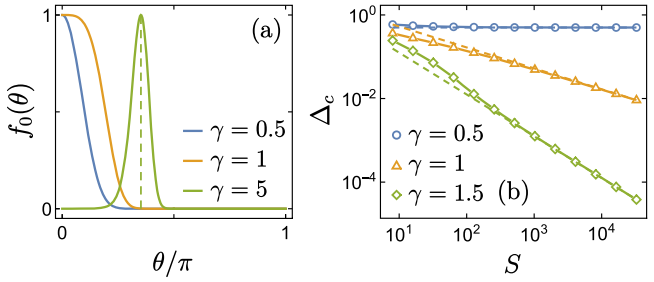

FIG. 3. (a) Steady-state quasiprobability distribution from the Fokker-Planck equation with $S = 20$. It is uniform along ϕ and peaked at $\theta = 0$ for $\gamma \leq 1$ and at the limit cycle (dashed line) for $\gamma > 1$. Their widths scale as $\Delta\theta \sim 1/\sqrt{S|1-\gamma|}$ for $\gamma \neq 1$ and $\Delta\theta \sim S^{-1/4}$ for $\gamma = 1$. (b) The decoherence rate Δ_c scales as S^0 for $\gamma < 1$ (fixed point), $S^{-1/2}$ for $\gamma = 1$ (bifurcation point), and S^{-1} for $\gamma > 1$ (limit cycle).

non-negative integers and λ_j are eigenvalues of the Jacobian matrix describing the linearized classical dynamics about the north pole [here $\lambda_j = -(1-\lambda) \pm \mathrm{i}$]. As we discuss later, this structure arises whenever the classical phase space has a stable fixed point. The corresponding eigenstates describe wave packets at different distances from the fixed point and are given by Laguerre polynomials for the spin model [36]. Here the wedge-shaped spectrum remains prominent for finite S [Fig. 2(c)].

Emergence of limit cycle—For $\gamma > 1$ the classical limit features an infinite number of equally spaced imaginary eigenvalues. The $\Lambda = 0$ state is spread uniformly along the limit cycle with a width $\Delta\theta \sim S^{-1/2}$ [Fig. 3(a)]. The other eigenstates of this branch are also clustered along the limit cycle, but with an additional phase winding $e^{\mathrm{i}l\phi}$. (The index l is the imaginary part of the eigenvalue and is a quantum number for this model [36].)

For any finite S this branch is parabolic, $\Lambda_l \approx \mathrm{i}l - (l^2/S)(\gamma^2 - 4\gamma + 5)/(2\gamma - 2)$ [36], so there is only a single state with a vanishing decay rate [Fig. 2(d)]. The curvature can be characterized by the real part Δ_c of the $l = 1$ member of the branch, which collapses as S^{-1} [Fig. 3(b)]. We argue later that the parabolic shape is responsible for diffusive broadening along the limit cycle as $\sqrt{t/S}$, which is suppressed for $S \to \infty$.

Besides the main branch, there is a series of parallel branches with decay rates $\approx n\Delta_p$ that are also distorted parabolically for finite S [Figs. 2(d) and 2(f)]. These eigenfunctions (with Hermite polynomial forms [36]) support wave packets at increasing distances from the limit cycle, and thus describe the approach to the limit cycle at a rate Δ_p, which has the classical value $2(\gamma-1)/\sqrt{\gamma}$ for $S \to \infty$ [Fig. 5(c)].

Figure 4 shows the quantum dynamics for $S = 50$ of an initially Gaussian quasiprobability distribution. The center of mass closely follows the classical trajectories as the wave packet approaches and orbits the limit cycle and then

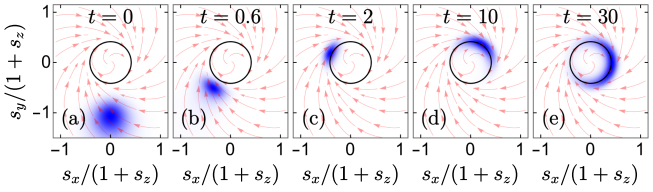

FIG. 4. (a)–(e) Dynamics of quasiprobability distribution in phase space from the Fokker-Planck equation with $S = 50$. The distribution is initially localized at the equator. Besides approaching the limit cycle as in the classical case, the quantum dynamics shows spreading along the limit cycle (dephasing).

slowly diffuses around it [40], losing phase coherence in the steady state due to the finite value of S.

Fixed point at south pole—The classical dynamics (1) for $\gamma > 1$ has a fixed point at $s_z = -1$ (south pole of the Bloch sphere), in addition to the limit cycle. In the Lindblad spectrum, we see this as an eigenvalue approaching 0 exponentially with S [36] such that there are two degenerate steady states for $S \to \infty$. [In Fig. 2(d) this state is too close to distinguish for $S = 300$ from the true steady state.] Furthermore, there is a whole set of eigenvalues governed by this fixed point which follow the $n_1\lambda_1 + n_2\lambda_2$ pattern characteristic of fixed points.

Bifurcation point: Emergence of algebraic decay—In Fig. 5(b) we show the low-lying spectrum at the Hopf bifurcation point $\gamma = 1$. These eigenvalues all collapse onto $\Lambda = \mathrm{i}l$ with decay rates $\sim S^{-1/2}$. Infinitely many eigenvalues become degenerate for $S \to \infty$ at every l, in contrast to the limit-cycle case where a single branch reaches the imaginary axis. Thus, for the same harmonic we get a superposition of an infinite number of eigenstates with different radial structures. It is this combination that allows an algebraic decay to the classical attractor. We explain this later in more detail for a generic (model-independent) setting. The width of the eigenstates scales as $S^{-1/4}$, as opposed to $S^{-1/2}$ for $\gamma \neq 1$ [Fig. 3(a)].

Dissipative Bose-Hubbard system—To verify the generality of our results, we have examined systems other than

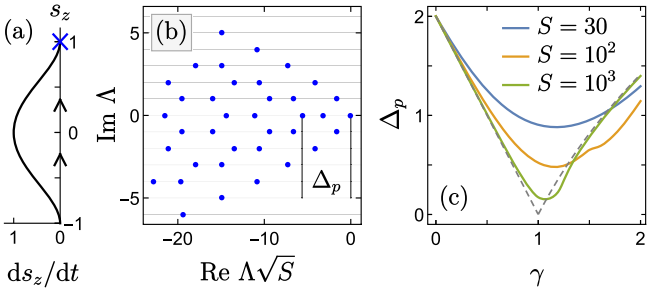

FIG. 5. (a) Classical flow and (b) the Lindblad spectrum for $S = 300$ at the Hopf bifurcation point, $\gamma = 1$. (c) Scaling of the gap Δ_p, defined in Figs. 2(c) and 2(d), showing "critical slowing down" at $\gamma = 1$.

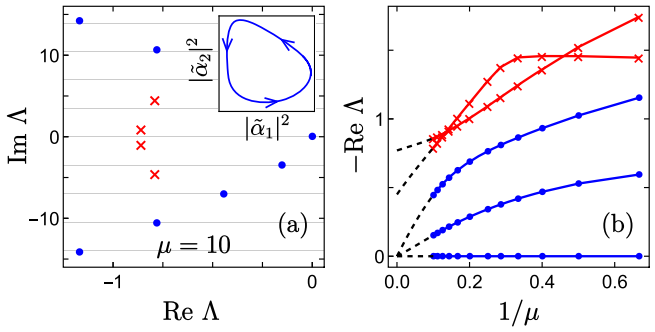

FIG. 6. Bose-Hubbard dimer in the limit-cycle regime. (a) Low-lying part of the spectrum. Inset: the limit cycle projected onto a plane in the four-dimensional phase space, where $|\tilde{\alpha}_{1,2}|^2$ are rescaled boson numbers in the two sites [36]. (b) In the classical limit $\mu \to \infty$ one branch (blue dots) has a vanishing decay rate, corresponding to the limit cycle, while all other eigenvalues (red crosses) stay in the left half plane.

the spin model. In Fig. 6 we show spectra and scalings for a dissipative Bose-Hubbard dimer. The model is that introduced in [33–35]; parameters are documented in [36]. The classical limit has a four-dimensional phase space, and there is no quantum number such as l for the spin model; hence, this system is qualitatively very different. The model has a parameter μ that controls the approach to the classical limit by tuning the average number of bosons. For a choice of parameters leading to a limit cycle in the classical limit, we observe the same signature of a branch collapsing onto the imaginary axis [Fig. 6(b)]. The branch follows a parabolic shape more closely as μ increases.

Generality—We have used specific models to demonstrate spectral signatures for three types of emergent classical behaviors (fixed points, limit cycles, and Hopf bifurcations). We now provide arguments and proofs that these signatures are generic and not model dependent.

In Figs. 2(e) and 2(f) eigenvalues corresponding to classical fixed points are given by $\Lambda = n_1\lambda_1 + n_2\lambda_2$, where $n_1, n_2 = 0, 1, 2, \ldots$ and $\lambda_{1,2}$ are eigenvalues of the linearized classical dynamics around the fixed point. This structure originates from the fact that at long times the dynamics occurs close to the fixed point, so the slow-decaying quantum eigenstates are peaked there, becoming infinitely localized in the classical limit [as in Fig. 3(a)]. Under such general conditions one can expand the quantum Fokker-Planck equation about the fixed point and keep the lowest-order terms, which gives a linear drift and a constant diffusion [36]. This system can be solved using a ladder-operator construction [41], yielding the eigenvalues $\Lambda = \sum_j n_j\lambda_j$, where $n_j = 0, 1, 2, \ldots$ and λ_j are eigenvalues of the classical Jacobian. Note that the same spectral form arises for quadratic Lindbladians [42].

The classical limit cycle is signaled by a branch that is purely imaginary and equally spaced, where each eigenstate is localized in the r direction and has a different ϕ harmonic, $e^{il\phi}$. This spectral structure is necessary to give rise to classical limit cycles. The azimuthal part of a quantum wave packet can be expanded as $g(\phi, t=0) = \sum_l c_l e^{-il\phi}$, with $l \in \mathbb{Z}$. For cycling dynamics, $g(\phi, t) = g(\phi - \omega t, 0) = \sum_l c_l e^{-il\phi} e^{il\omega t}$. Since a state with eigenvalue Λ contributes a factor $e^{\Lambda t}$ to the dynamics, this implies that the eigenvalues are $\Lambda_l = il\omega$ and the eigenfunctions have the angular form $\sim e^{-il\phi}$. To reproduce a sharp point on a classical trajectory, all Fourier modes (each $l \in \mathbb{Z}$) must be present.

Close to the classical limit the branch is parabolic. This leads to $g(\phi, t) = \sum_l c_l e^{-il(\phi-\omega t)} e^{-l^2 t/\tau} \sim e^{\tau(\phi-\omega t)^2/4t}$, where $\tau \to \infty$ in the classical limit. Hence, the wave packet broadens as $\Delta\phi \sim \sqrt{t/\tau}$. Such diffusive spreading, expected from the diffusion term in the Fokker-Planck equation, is thus coupled to the parabolic distortion of the branch, which should be generic.

Close to the limit cycle a classical trajectory has a vanishing radial speed, $\dot{r} \to 0$, but a nonzero angular speed, $r\dot{\phi} \to r_{\rm lc}\dot{\phi}$. This decoupling of timescales produces many quasistationary (slow-decaying) orbits at small distances from the limit cycle, which show up in the spectrum as additional branches. Note that these branches are absent for a fixed point where the radial and angular speeds decay proportionally.

Finally, we reported above that the classical bifurcation point involves many quantum eigenvalues corresponding to the same harmonic, and hence different r structures, collapsing onto the imaginary axis. This enables the characteristic algebraic decay, as $\langle r\rangle = \sum_n c_n \langle r\rangle_n e^{-\xi_n t/\sqrt{S}}$ is now obtained as an infinite sum over vanishing decay rates ($n = 0, 1, 2, \ldots$). Here, c_n define the initial state in terms of eigenstate overlaps, $\langle r\rangle_n$ are the eigenstate expectation values of the radial coordinate, and $-\xi_n/\sqrt{S}$ are the eigenvalues. (The values of c_n and $\langle r\rangle_n$ depend on the normalization of the left and right eigenstates, but their product is uniquely defined.) In general, power-law scalings of these quantities with n can give rise to algebraic decay; the specific scalings are likely system dependent. In the spin model, $\xi_n \sim n^{3/2}$, and for a localized initial state, this leads to $\langle r\rangle \sim t^{-1/2}$, as detailed in the Supplemental Material [36].

For a Hopf bifurcation, generically $\dot{r}/(r\dot{\phi}) \sim r$ vanishes close to the classical attractor. Thus, we again have a dynamical decoupling of radial and angular motion. The quasistationary orbits at small r have the same angular frequency, which implies that the imaginary parts of the low-lying eigenvalues are equally spaced.

A generic system might be expected to have several fixed points and/or limit cycles. Our observation for the spin system at $\gamma > 1$ [Fig. 2(f)] suggests that each such feature governs a collection of eigenvalues in the corresponding quantum Liouvillian spectrum.

Context and discussion—We have initiated the study of the spectral origin of nonlinear dynamical phenomena in

the classical limit of quantum dissipative physics. Such classical limits are useful for understanding physical phenomena in different setups [38–40,43–65]. We have elucidated the prototypical cases of fixed points, limit cycles, and critical slowing down. While such phenomena have been predicted in quantum systems using semiclassical equations of motion, this Letter provides a foundation for how they arise from the full quantum generator.

Algebraic decay has previously been seen for the thermodynamic limit [66–71]. Here, we illustrate the general mechanism of algebraic decay in the classical limit, as also observed in Ref. [72]. Our findings regarding the spectral signatures of a limit cycle should also apply to other open quantum systems that support limit cycles in the classical limit, e.g., a quantum Van der Pol oscillator [52,53,56,57,73], an open Dicke model [44,58,61,74], and others [75–77]. We have shown how the apporach of an infinite number of eigenvalues to the imaginary axis provides mechanisms for both limit-cycle dynamics and algebraic decay in the classical limit. Liouvillian eigenvalues located on or approaching the imaginary axis have also been studied from other perspectives [31,59,71,78–95].

Our results open up several research directions and questions: (1) It remains to be explained how other classical nonlinear phenomena, particularly period doubling to chaos, emerges from Liouvillian spectra [65]. (2) How do the spectra of Liouvillian maps (confined to the unit circle rather than the negative half plane) lead to discrete-time nonlinear phenomena [50]? (3) Can one connect classical nonlinear phenomena to statistical aspects of the Liouvillian spectra, analogous to the Bohigas-Giannoni-Schmit conjecture [10] for the Hamiltonian case?

Acknowledgments—We thank Nigel Cooper, Jonathan Dubois, and Felix Fritzsch for useful discussions. This work was supported in part by the Deutsche Forschungsgemeinschaft through SFB 1143 (Project ID 247310070).

[1] P. Ehrenfest, Bemerkung über die angenäherte Gültigkeit der klassischen Mechanik innerhalb der Quantenmechanik, Z. Phys. **45**, 455 (1927).
[2] K. Hepp, The classical limit for quantum mechanical correlation functions, Commun. Math. Phys. **35**, 265 (1974).
[3] L. G. Yaffe, Large N limits as classical mechanics, Rev. Mod. Phys. **54**, 407 (1982).
[4] L. E. Reichl and W. A. Lin, The search for a quantum KAM theorem, Found. Phys. **17**, 689 (1987).
[5] M. C. Gutzwiller, *Chaos in Classical and Quantum Mechanics* (Springer, New York, 1990), 10.1007/978-1-4612-0983-6.
[6] W. H. Zurek, Decoherence and the transition from quantum to classical, Phys. Today **44**, No. 10, 36 (1991).
[7] W. H. Zurek, Decoherence, einselection, and the quantum origins of the classical, Rev. Mod. Phys. **75**, 715 (2003).
[8] M. A. Schlosshauer, *Decoherence and the Quantum-To-Classical Transition* (Springer, New York, 2007), 10.1007/978-3-540-35775-9.
[9] U. Klein, What is the limit $\hbar \to 0$ of quantum theory?, Am. J. Phys. **80**, 1009 (2012).
[10] O. Bohigas, M. J. Giannoni, and C. Schmit, Characterization of chaotic quantum spectra and universality of level fluctuation laws, Phys. Rev. Lett. **52**, 1 (1984).
[11] D. T. Robb and L. E. Reichl, Chaos in a two-spin system with applied magnetic field, Phys. Rev. E **57**, 2458 (1998).
[12] J. Emerson and L. E. Ballentine, Characteristics of quantum-classical correspondence for two interacting spins, Phys. Rev. A **63**, 052103 (2001).
[13] S. Müller, S. Heusler, P. Braun, F. Haake, and A. Altland, Semiclassical foundation of universality in quantum chaos, Phys. Rev. Lett. **93**, 014103 (2004).
[14] S. Müller, S. Heusler, A. Altland, P. Braun, and F. Haake, Periodic-orbit theory of universal level correlations in quantum chaos, New J. Phys. **11**, 103025 (2009).
[15] M. A. Bastarrachea-Magnani, S. Lerma-Hernández, and J. G. Hirsch, Comparative quantum and semiclassical analysis of atom-field systems. II. Chaos and regularity, Phys. Rev. A **89**, 032102 (2014).
[16] G. Nakerst and M. Haque, Chaos in the three-site Bose-Hubbard model: Classical versus quantum, Phys. Rev. E **107**, 024210 (2023).
[17] L. Benet, F. Borgonovi, F. M. Izrailev, and L. F. Santos, Quantum-classical correspondence of strongly chaotic many-body spin models, Phys. Rev. B **107**, 155143 (2023).
[18] J. Novotný and P. Stránský, Relative asymptotic oscillations of the out-of-time-ordered correlator as a quantum chaos indicator, Phys. Rev. E **107**, 054220 (2023).
[19] J. Chávez-Carlos, B. López-del Carpio, M. A. Bastarrachea-Magnani, P. Stránský, S. Lerma-Hernández, L. F. Santos, and J. G. Hirsch, Quantum and classical Lyapunov exponents in atom-field interaction systems, Phys. Rev. Lett. **122**, 024101 (2019).
[20] M. Rautenberg and M. Gärttner, Classical and quantum chaos in a three-mode bosonic system, Phys. Rev. A **101**, 053604 (2020).
[21] S. Pappalardi, A. Polkovnikov, and A. Silva, Quantum echo dynamics in the Sherrington-Kirkpatrick model, SciPost Phys. **9**, 21 (2020).
[22] A. Lerose and S. Pappalardi, Bridging entanglement dynamics and chaos in semiclassical systems, Phys. Rev. A **102**, 032404 (2020).
[23] L. E. Reichl, *The Transition to Chaos: Conservative Classical Systems and Quantum Manifestations*, 3rd ed. (Springer, New York, 2021), 10.1007/978-3-030-63534-3.
[24] S. Strogatz, *Nonlinear Dynamics and Chaos: With Applications to Physics, Biology, Chemistry, and Engineering*, 2nd ed. (CRC Press, Boca Raton, 2018).
[25] R. Hilborn, *Chaos and Nonlinear Dynamics: An Introduction for Scientists and Engineers* (Oxford University Press, New York, 2000).
[26] G. Lindblad, On the generators of quantum dynamical semigroups, Commun. Math. Phys. **48**, 119 (1976).
[27] V. Gorini, A. Kossakowski, and E. C. G. Sudarshan, Completely positive dynamical semigroups of N-level systems, J. Math. Phys. (N.Y.) **17**, 821 (1976).

[28] H. Breuer and F. Petruccione, *The Theory of Open Quantum Systems* (Oxford University Press, New York, 2002).

[29] D. E. Evans, Irreducible quantum dynamical semigroups, Commun. Math. Phys. **54**, 293 (1977).

[30] B. Buča and T. Prosen, A note on symmetry reductions of the Lindblad equation: Transport in constrained open spin chains, New J. Phys. **14**, 073007 (2012).

[31] V. V. Albert and L. Jiang, Symmetries and conserved quantities in Lindblad master equations, Phys. Rev. A **89**, 022118 (2014).

[32] Z. Zhang, J. Tindall, J. Mur-Petit, D. Jaksch, and B. Buča, Stationary state degeneracy of open quantum systems with non-Abelian symmetries, J. Phys. A **53**, 215304 (2020).

[33] A. Giraldo, B. Krauskopf, N. G. Broderick, J. A. Levenson, and A. M. Yacomotti, The driven-dissipative Bose–Hubbard dimer: Phase diagram and chaos, New J. Phys. **22**, 043009 (2020).

[34] A. Giraldo, N. G. Broderick, and B. Krauskopf, Chaotic switching in driven-dissipative Bose-Hubbard dimers: When a flip bifurcation meets a T-point in $\mathbb{R}^4$, Discret. Contin. Dyn. Syst. Ser. B **27**, 4023 (2022).

[35] A. Giraldo, S. J. Masson, N. G. Broderick, and B. Krauskopf, Semiclassical bifurcations and quantum trajectories: A case study of the open Bose–Hubbard dimer, Eur. Phys. J. Spec. Top. **231**, 385 (2022).

[36] See Supplemental Material at http://link.aps.org/supplemental/10.1103/PhysRevLett.134.050407, which includes Ref. [37], for an overview of the Fokker-Planck formulation, eigenstates of the spin model in the classical limit, animations of the spin model on the Bloch sphere, a derivation of the universal spectrum for a fixed point, a parabolic distortion of the limit-cycle branch from perturbation theory, emergence of the algebraic decay from the spectrum, and parameters for the Bose-Hubbard dimer.

[37] A. Ronveaux and F. M. Arscott, *Heun's Differential Equations* (Oxford University Press, New York, 1995).

[38] W. T. Strunz and I. C. Percival, Classical mechanics from quantum state diffusion-a phase-space approach, J. Phys. A **31**, 1801 (1998).

[39] J. Dubois, U. Saalmann, and J. M. Rost, Semi-classical Lindblad master equation for spin dynamics, J. Phys. A **54**, 235201 (2021).

[40] C. M. Savage, Oscillations and quantized second-harmonic generation, Phys. Rev. A **37**, 158 (1988).

[41] T. K. Leen, R. Friel, and D. Nielsen, Eigenfunctions of the multidimensional linear noise Fokker-Planck operator via ladder operators, arXiv:1609.01194.

[42] T. Prosen and T. H. Seligman, Quantization over boson operator spaces, J. Phys. A **43**, 392004 (2010).

[43] M. A. Armen and H. Mabuchi, Low-lying bifurcations in cavity quantum electrodynamics, Phys. Rev. A **73**, 063801 (2006).

[44] M. J. Bhaseen, J. Mayoh, B. D. Simons, and J. Keeling, Dynamics of nonequilibrium Dicke models, Phys. Rev. A **85**, 013817 (2012).

[45] T. E. Lee and H. R. Sadeghpour, Quantum synchronization of quantum van der Pol oscillators with trapped ions, Phys. Rev. Lett. **111**, 234101 (2013).

[46] N. Lörch, J. Qian, A. Clerk, F. Marquardt, and K. Hammerer, Laser theory for optomechanics: Limit cycles in the quantum regime, Phys. Rev. X **4**, 011015 (2014).

[47] T. E. Lee, C.-K. Chan, and S. Wang, Entanglement tongue and quantum synchronization of disordered oscillators, Phys. Rev. E **89**, 022913 (2014).

[48] S. Walter, A. Nunnenkamp, and C. Bruder, Quantum synchronization of two Van der Pol oscillators, Ann. Phys. (Berlin) **527**, 131 (2014).

[49] A. Roulet and C. Bruder, Synchronizing the smallest possible system, Phys. Rev. Lett. **121**, 053601 (2018).

[50] R. R. W. Wang, B. Xing, G. G. Carlo, and D. Poletti, Period doubling in period-one steady states, Phys. Rev. E **97**, 020202(R) (2018).

[51] J. S. Ferreira and P. Ribeiro, Lipkin-Meshkov-Glick model with Markovian dissipation: A description of a collective spin on a metallic surface, Phys. Rev. B **100**, 184422 (2019).

[52] S. Dutta and N. R. Cooper, Critical response of a quantum van der Pol oscillator, Phys. Rev. Lett. **123**, 250401 (2019).

[53] W.-K. Mok, L.-C. Kwek, and H. Heimonen, Synchronization boost with single-photon dissipation in the deep quantum regime, Phys. Rev. Res. **2**, 033422 (2020).

[54] B. Fernengel and B. Drossel, Bifurcations and chaos in nonlinear Lindblad equations, J. Phys. A **53**, 385701 (2020).

[55] D. Huybrechts, F. Minganti, F. Nori, M. Wouters, and N. Shammah, Validity of mean-field theory in a dissipative critical system: Liouvillian gap, $\mathbb{PT}$-symmetric antigap, and permutational symmetry in the XYZ model, Phys. Rev. B **101**, 214302 (2020).

[56] L. Ben Arosh, M. C. Cross, and R. Lifshitz, Quantum limit cycles and the Rayleigh and van der Pol oscillators, Phys. Rev. Res. **3**, 013130 (2021).

[57] N. Thomas and M. Senthilvelan, Quantum synchronization in quadratically coupled quantum van der Pol oscillators, Phys. Rev. A **106**, 012422 (2022).

[58] K. C. Stitely, A. Giraldo, B. Krauskopf, and S. Parkins, Nonlinear semiclassical dynamics of the unbalanced, open Dicke model, Phys. Rev. Res. **2**, 033131 (2020).

[59] K. Seibold, R. Rota, and V. Savona, Dissipative time crystal in an asymmetric nonlinear photonic dimer, Phys. Rev. A **101**, 033839 (2020).

[60] Y. Kato and H. Nakao, Turing instability in quantum activator–inhibitor systems, Sci. Rep. **12**, 15573 (2022).

[61] J. Li, R. Fazio, and S. Chesi, Nonlinear dynamics of the dissipative anisotropic two-photon Dicke model, New J. Phys. **24**, 083039 (2022).

[62] L. R. Bakker, M. S. Bahovadinov, D. V. Kurlov, V. Gritsev, A. K. Fedorov, and D. O. Krimer, Driven-dissipative time crystalline phases in a two-mode bosonic system with Kerr nonlinearity, Phys. Rev. Lett. **129**, 250401 (2022).

[63] L. Zhang, Z. Wang, Y. Wang, J. Zhang, Z. Wu, J. Jie, and Y. Lu, Quantum synchronization of a single trapped-ion qubit, Phys. Rev. Res. **5**, 033209 (2023).

[64] P. Kongkhambut, J. Skulte, L. Mathey, J. G. Cosme, A. Hemmerich, and H. Keßler, Observation of a continuous time crystal, Science **377**, 670 (2022).

[65] J. Li and S. Chesi, Routes to chaos in the balanced two-photon Dicke model with qubit dissipation, Phys. Rev. A **109**, 053702 (2024).

[66] A. Tomadin, S. Diehl, and P. Zoller, Nonequilibrium phase diagram of a driven and dissipative many-body system, Phys. Rev. A **83**, 013611 (2011).
[67] Z. Cai and T. Barthel, Algebraic versus exponential decoherence in dissipative many-particle systems, Phys. Rev. Lett. **111**, 150403 (2013).
[68] M. Žnidarič, Relaxation times of dissipative many-body quantum systems, Phys. Rev. E **92**, 042143 (2015).
[69] M. V. Medvedyeva and S. Kehrein, Power-law approach to steady state in open lattices of noninteracting electrons, Phys. Rev. B **90**, 205410 (2014).
[70] F. Vicentini, F. Minganti, R. Rota, G. Orso, and C. Ciuti, Critical slowing down in driven-dissipative Bose-Hubbard lattices, Phys. Rev. A **97**, 013853 (2018).
[71] F. Minganti, I. I. Arkhipov, A. Miranowicz, and F. Nori, Liouvillian spectral collapse in the Scully-Lamb laser model, Phys. Rev. Res. **3**, 043197 (2021).
[72] D. Poletti, J.-S. Bernier, A. Georges, and C. Kollath, Interaction-induced impeding of decoherence and anomalous diffusion, Phys. Rev. Lett. **109**, 045302 (2012).
[73] A. Cabot, G. L. Giorgi, and R. Zambrini, Nonequilibrium transition between dissipative time crystals, PRX Quantum **5**, 030325 (2024).
[74] X. Nie and W. Zheng, Mode softening in time-crystalline transitions of open quantum systems, Phys. Rev. A **107**, 033311 (2023).
[75] C.-K. Chan, T. E. Lee, and S. Gopalakrishnan, Limit-cycle phase in driven-dissipative spin systems, Phys. Rev. A **91**, 051601(R) (2015).
[76] F. Piazza and H. Ritsch, Self-ordered limit cycles, chaos, and phase slippage with a superfluid inside an optical resonator, Phys. Rev. Lett. **115**, 163601 (2015).
[77] J. Skulte, P. Kongkhambut, H. Keßler, A. Hemmerich, L. Mathey, and J. G. Cosme, Realizing limit cycles in dissipative bosonic systems, Phys. Rev. A **109**, 063317 (2024).
[78] B. Baumgartner and H. Narnhofer, Analysis of quantum semigroups with GKS–Lindblad generators: II. General, J. Phys. A **41**, 395303 (2008).
[79] V. V. Albert, B. Bradlyn, M. Fraas, and L. Jiang, Geometry and response of Lindbladians, Phys. Rev. X **6**, 041031 (2016).
[80] F. Iemini, A. Russomanno, J. Keeling, M. Schirò, M. Dalmonte, and R. Fazio, Boundary time crystals, Phys. Rev. Lett. **121**, 035301 (2018).
[81] B. Buča, J. Tindall, and D. Jaksch, Non-stationary coherent quantum many-body dynamics through dissipation, Nat. Commun. **10**, 1730 (2019).
[82] B. Buča and D. Jaksch, Dissipation induced nonstationarity in a quantum gas, Phys. Rev. Lett. **123**, 260401 (2019).
[83] C. Booker, B. Buča, and D. Jaksch, Non-stationarity and dissipative time crystals: Spectral properties and finite-size effects, New J. Phys. **22**, 085007 (2020).
[84] L. F. dos Prazeres, L. da Silva Souza, and F. Iemini, Boundary time crystals in collective d-level systems, Phys. Rev. B **103**, 184308 (2021).
[85] B. Buča, C. Booker, and D. Jaksch, Algebraic theory of quantum synchronization and limit cycles under dissipation, SciPost Phys. **12**, 097 (2022).
[86] H. Alaeian and B. Buča, Exact multistability and dissipative time crystals in interacting fermionic lattices, Commun. Phys. **5**, 318 (2022).
[87] K. Seibold, R. Rota, F. Minganti, and V. Savona, Quantum dynamics of dissipative Kerr solitons, Phys. Rev. A **105**, 053530 (2022).
[88] J. Dubois, U. Saalmann, and J. M. Rost, Symmetry-induced decoherence-free subspaces, Phys. Rev. Res. **5**, L012003 (2023).
[89] L. da Silva Souza, L. F. dos Prazeres, and F. Iemini, Sufficient condition for gapless spin-boson Lindbladians, and its connection to dissipative time crystals, Phys. Rev. Lett. **130**, 180401 (2023).
[90] J. Tindall, D. Jaksch, and C. S. Muñoz, On the generality of symmetry breaking and dissipative freezing in quantum trajectories, SciPost Phys. Core **6**, 004 (2023).
[91] X. Li, Y. Li, and J. Jin, Synchronization of persistent oscillations in spin systems with nonlocal dissipation, Phys. Rev. A **107**, 032219 (2023).
[92] Y. Li, X. Li, and J. Jin, Quantum nonstationary phenomena of spin systems in collision models, Phys. Rev. A **107**, 042205 (2023).
[93] Y. Nakanishi and T. Sasamoto, Dissipative time crystals originating from parity-time symmetry, Phys. Rev. A **107**, L010201 (2023).
[94] M. Krishna, P. Solanki, M. Hajdušek, and S. Vinjanampathy, Measurement-induced continuous time crystals, Phys. Rev. Lett. **130**, 150401 (2023).
[95] F. Iemini, D. Chang, and J. Marino, Dynamics of inhomogeneous spin ensembles with all-to-all interactions: Breaking permutational invariance, Phys. Rev. A **109**, 032204 (2024).